NANO LETTERS

2007
Vol. 7, No. 6
1556−1560

Ultra-Large-Scale Directed Assembly of Single-Walled Carbon Nanotube Devices

Aravind Vijayaraghavan,[†] Sabine Blatt,[†] Daniel Weissenberger,[‡] Matti Oron-Carl,[†] Frank Hennrich,[†] Dagmar Gerthsen,[‡] Horst Hahn,[†] and Ralph Krupke*,[†]

Institut für Nanotechnologie, Forschungszentrum Karlsruhe, D-76021 Karlsruhe, Germany, and Laboratorium für Elektronenmikroskopie, Universität Karlsruhe, D-76128 Karlsruhe, Germany.

Received February 15, 2007; Revised Manuscript Received April 13, 2007

ABSTRACT

One of the biggest limitations of conventional carbon nanotube device fabrication techniques is the inability to scale up the processes to fabricate a large number of devices on a single chip. In this report, we demonstrate the directed and precise assembly of single-nanotube devices with an integration density of several million devices per square centimeter, using a novel aspect of nanotube dielectrophoresis. We show that the dielectrophoretic force fields change incisively as nanotubes assemble into the contact areas, leading to a reproducible directed assembly which is self-limiting in forming single-tube devices. Their functionality has been tested by random sampling of device characteristics using microprobes.

In the 10 years since the first electronic transport measurements were performed on individual single-walled carbon nanotubes (SWNTs),[1] tremendous progress has been made in understanding their electronic structure and its influence on their electronic transport properties.[2] Subsequently, a number of applications for nanotubes have been proposed, ranging from basic microelectronic components like interconnects[3] and field-effect transistors,[4] to more exotic applications such as single-electron transistors[5] and superconductors.[6] Still, the fundamental issue of device fabrication remains the biggest challenge for effective commercialization of nanotube electronics. In an ideal situation, it is desirable to position a single nanotube precisely at a predefined location and orientation, preferably bridging the ends of two metallic leads, resulting in a robust device. Furthermore, it should be possible to scale up the fabrication technique to simultaneously and reproducibly fabricate a very large number of such devices on a single chip, each accessible individually for electronic transport. Conventional nanotube growth and device fabrication techniques using chemical vapor deposition or spin-casting are unable to achieve this, due to a lack of precise control over nanotube positioning and orientation.[2,7] Some advances have been made in directed growth or assembly of individual nanotubes on a substrate.[8,9] However, methods involving high-temperature processes like chemical vapor deposition or chemical modifications of the substrate are often incompatible with microelectronic fabrication technologies.

Recently, radio frequency (rf) dielectrophoresis has been used to assemble a small number of devices of individual or bundled carbon nanotubes[10−12] and nanowires,[13] by moving these one-dimensional nanoscale objects in inhomogeneous electric fields. In previous reports,[11,12] including our own, a self-limiting single-nanotube assembly has been observed at the electrode gap under specific deposition conditions. The widely accepted mechanism for this phenomenon is the short-circuiting of the electrodes by the contacted object. In this report, we will show using impedance spectroscopy that this mechanism cannot explain the formation of single-tube devices. Backed by finite-element simulations, we present an alternate and more universal mechanism that involves redistribution of the electric field around the deposited nanotube in the electrode gap.

The high density of individually accessible devices is made possible by the scalability of the capacitively coupled electrodes used in this deposition scheme. This, in combination with the new understanding of self-limiting single-nanotube assembly, offers the only method available yet to meet the goals of large-scale directed and precise assembly of functional single-nanotube devices with densities beyond several million devices per square centimeter, which is also fully compatible with silicon-based microelectronics fabrication technologies and all forms of pre- and postprocessing of the nanotubes and devices.

Figure 1 shows a schematic of the electrode arrangement and nanotube deposition. The important feature of our setup

* Corresponding author. ralph.krupke@int.fzk.de.
[†] Institut für Nanotechnologie, Forschungszentrum Karlsruhe.
[‡] Laboratorium für Elektronenmikroskopie, Universität Karlsruhe.

10.1021/nl0703727 CCC: $37.00
Published on Web 05/08/2007

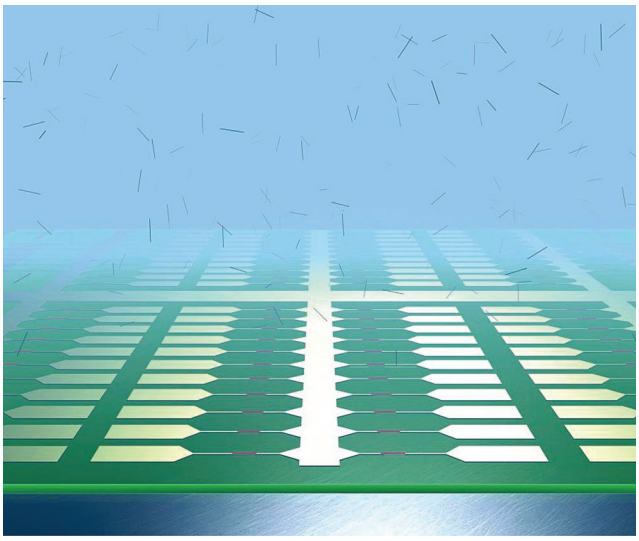

Figure 1. Schematic of the high-density array of single-tube devices, comprising interconnected biased electrodes and counter electrodes (yellow) which are capacitively coupled to the p-type silicon substrate (gray) via 800 nm of SiO_2 (green). Individual single-walled carbon nanotubes (black) dispersed in aqueous surfactant solution (blue) form single-tube devices (magenta) at a density of several million per square centimeter due to self-limiting dielectrophoretic assembly onto each of the 0.8 μm wide electrode gaps.

is that only one of the surface electrodes (biased electrode, BE) is connected directly to the rf source. The other electrode of each device is a floating counter electrode (CE). The rf signal is applied between the BE and the underlying silicon gate electrode (GE). For high electric-field frequencies (ω_d > 100 kHz), the impedance of the CE/SiO_2/GE structure ($1/j\omega_d C_{CE-GE}$) reduces significantly. The CE is now capacitively coupled to the GE and acquires a similar potential as that of the GE. This allows us to bias all the distinct CEs without having to bond wires individually to each. This capacitive coupling, however, is not a prerequisite for the self-limiting deposition of single nanotubes, as we will discuss later.

The overall dimensions of a nanotube device are limited by the dimensions of the contacting electrodes (source and drain) rather than the dimensions of the nanotube itself. Biasing the CE by capacitive coupling allows us to reduce the dimensions of the CE, thereby increasing the density of electrode pairs that can be accommodated in any given area of the chip. A capacitively coupled CE cannot be shrunk to arbitrarily small dimensions. Below a critical areal size A_{CE}, at a given oxide thickness t_{SiO_2}, the capacitance between the CE and the underlying GE ($C_{CE-G} = \xi_o \xi_{r-SiO_2} A_{CE}/t_{SiO_2}$) becomes too small and the coupling between the CE and GE too weak for attaining a sufficient potential difference between the BE and CE. Using a series of depositions with different CE dimensions (see Supporting Information), $A_{CE} \approx 10\ \mu m^2$ was determined as the lower limit for effective nanotube deposition on a 800 nm thick oxide layer. Within this limit, an electrode array consisting of 100 electrode pairs could be fabricated in a 100 μm × 100 μm area on the substrate, as seen in Figure 1. One electrode of each pair was connected together and to a large surface bonding pad,

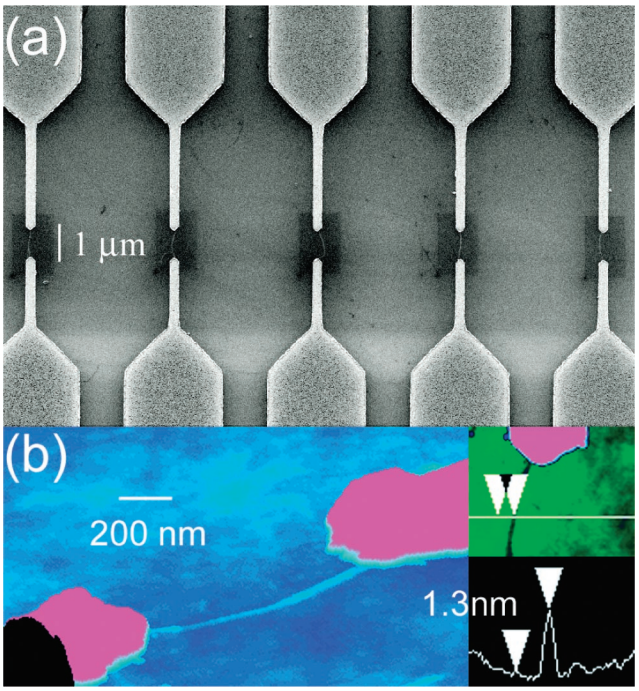

Figure 2. (a) Zoom-in of the electrode array showing five adjacent devices, with each electrode pair bridged by one carbon nanotube, visible as fine white lines within the dark central areas. The dark areas are due to contrast enhancement while scanning the zoomed-in area around each device.[25] (b) Atomic force microscopy image of one such device. The height profile confirms the bridging by an individual nanotube.

such that a single surface electrical contact can be used to bias all the BEs. Similarly, a single electrical contact to the underlying conducting substrate is used to bias all the CEs via capacitive coupling.

The directed assembly of nanotubes is performed in a simple experimental setup under ambient conditions (Supporting Information). Scanning electron microscopy (SEM) and atomic force microscopy (AFM) were used to count and image the deposited nanotubes. Figure 2a shows the bridging of five adjacent electrode pairs fabricated with the above scheme, which is representative of the whole array. Most of the electrode pairs were bridged by one individual nanotube or small bundle, as verified by AFM in Figure 2b. This represents a density of a few hundred thousand devices per cm^2. Some of the electrode pairs had nanotubes connected to one or both electrodes, but not bridging them. This is expected, since the length distribution of the dispersed nanotubes extends from 200 nm to 2 μm and a significant number of nanotubes are not long enough to span the entire gap, which is only 0.8 μm wide. Using suspensions with uniform nanotube length or using narrower electrode gaps, we can increase the yield of bridged electrodes. Only about 10% of the electrodes were bridged by multiple nanotubes.

The extent of coupling between the counter electrode and the substrate depends not only on A_{CE} but also on t_{SiO_2}. The capacitance (C_{CE-G}) has a limiting value, below which the impedance becomes too high for efficient coupling. For the electrode arrangement and rf amplitude given above, this value is approximately 0.5 fF. If we decrease the electrode

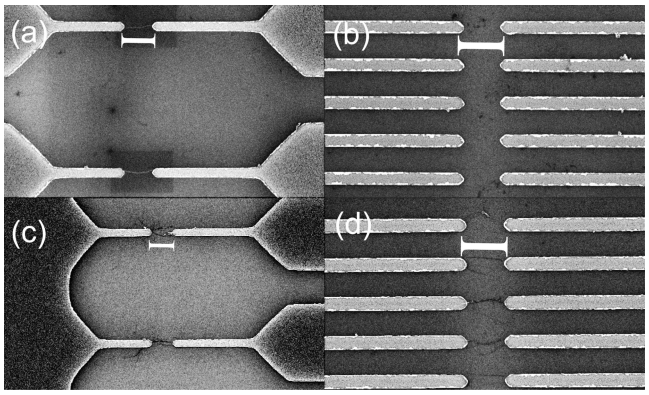

Figure 3. Effect of oxide thickness and counter electrode area on the directed assembly of nanotube devices, in terms of number of bridging nanotubes per electrode pair. (a) Single nanotubes assembled for 800 nm thick oxide layer and 10 μm^2 counter electrode area. (b) No nanotubes assembled for 800 nm oxide and 1 μm^2 electrode area. (c) Few nanotubes assembled for 50 nm oxide and 10 μm^2 electrode area. (d) One or two nanotubes assembled for 50 nm oxide and 1 μm^2 electrode area. Scale bars equal 1 μm in all images.

area, the oxide thickness has to decrease correspondingly, to maintain the same capacitive coupling. By decreasing t_{SiO_2} it is possible to improve the coupling for smaller electrodes than previously described. Two chips with $t_{SiO_2} = 800$ and 50 nm, each with $A_{CE} = 10\ \mu m^2$ and 1 μm^2, were tested for device array fabrication. Figure 3 shows SEM images of these, after nanotube deposition. It can be seen that the electrodes with $A_{CE} = 1\ \mu m^2$ have no nanotubes for $t_{SiO_2} =$ 800 nm but one or two for $t_{SiO_2} = 50$ nm. Similarly, the electrodes with $A_{CE} = 10\ \mu m^2$ have one nanotube for $t_{SiO_2} =$ 800 nm but a few for $t_{SiO_2} = 50$ nm. By optimizing the oxide thickness and rf amplitude, it is possible to improve the device density further, while limiting the nanotubes to one per device. For instance the chip with 1 μm^2 electrodes has 400 electrode pairs in a 100 $\mu m \times 100\ \mu m$ area, of which more then 90% were bridged, giving an even higher density of 3−4 million functional nanotube devices per cm^2. This is comparable to the current level of integration complexity in microelectronics, namely, ultra-large-scale integration (ULSI), which specifies at least 1 million transistors per chip.

We now discuss the important observation that under optimum conditions the number of nanotubes or bundles deposited across the electrode gaps is limited to one. At first sight, the deposition of a nanotube in the gap would appear to "short-circuit" the electrodes, equalizing their potentials, thereby limiting further nanotube deposition. However, this mechanism, proposed earlier,[10,11] requires nanotube contact resistances which are low compared to the impedance of the $CE/SiO_2/GE$ structure and the suspension. Supplementary Figure 2 shows impedance spectroscopy measurements of single-tube devices before and after dielectrophoretic nanotube deposition. Before deposition, the impedance of the gap between the tips of the BE and CE is ohmic, purely due to the ionic conductivity σ of the suspension. Helmholtz double layer formation at the metal−suspension interface is absent at $\omega = 300$ kHz, as expected from the ionic charge relaxation frequency $\tau^{-1} = \sigma/\epsilon \approx 200$ kHz (with $\sigma = 0.1$ S/m and

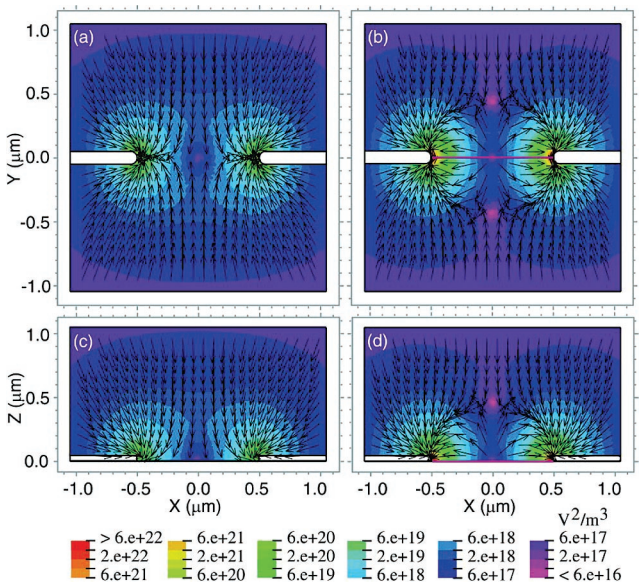

Figure 4. Simulation of dielectrophoretic force fields. Simulated map of ∇E^2 in a volume around the electrodes for two orthogonal cross sections. (a, b) ∇E^2 at the surface of the substrate ($X-Y$ plane at $Z = 0$). (c, d) ∇E^2 perpendicular to the substrate ($X-Z$ plane at $Y = 0$). The arrows indicate the direction of the force acting on a highly polarizable nanotube−surfactant hybrid and, hence, the direction of nanotube motion. The background color is the magnitude of ∇E^2. The dielectrophoretic force is attractive in all regions in the absence of deposited nanotubes (a, c), while the force becomes repulsive between the electrodes, once a nanotube (magenta line) has been deposited (b, d).

permittivity $\epsilon \approx 85\epsilon_0$). Hence, the potential drops uniformly between the electrodes and results in a strong alternating nonuniform electric field between the electrode tips, giving rise to a dielectrophoretic force which attracts the first nanotube to deposit between them. Since the impedance of a device (nanotube and its contact resistances) is significantly higher than either the impedance of the suspension or of the $CE/SiO_2/GE$ structure, the impedance of the gap under deposition conditions is similar before and after a nanotube is deposited. Consequently, the potential difference across the electrodes does not reduce upon nanotube deposition and, therefore, a new explanation for the self-limiting deposition is sought. We propose that the first deposited nanotube changes the local electric potential distribution such that further nanotube deposition is inhibited, despite the electrode potentials not equalizing.

We have performed numerical simulations of the dielectrophoretic forces in the vicinity of the electrodes using a finite element partial differential equations solver (FlexPDE). Details of the simulation are available in the Supporting Information. Supplementary Figure 3 compares the simulated potential drop between the electrodes in the absence and presence of a nanotube. It is known that if a nanotube bridges the electrodes, the contact resistance of the two nanotube−metal junctions causes the potential to drop primarily within 5 nm into the nanotube.[14,15] As a result, in the presence of a nanotube, the region between the electrodes is nearly field-free. The gradient of the square of the electric field (∇E^2) is a measure of the dielectrophoretic force experienced by a

nanotube,[16] provided the Clausius−Mosotti factor (CMF) accounting for the screened polarizability of the nanotube in the aqueous solutions is known. Figure 4 shows maps of the simulated ∇E^2, the dielectrophoretic force field, before and after nanotube deposition. Under the condition used, CMF is positive for both metallic and semiconducting carbon nanotubes.[16] Hence the direction of ∇E^2 (arrows in Figure 4) is identical to the direction of dielectrophoretic nanotube motion for all nanotubes. Before any nanotube is deposited, nanotubes experience attractive forces toward the gap at all points, directing a nanotube to deposit between the electrodes. However once a nanotube has been deposited, the dielectrophoretic force-field changes incisively and the region at and around the nanotube develops strong repulsive forces, preventing further nanotube deposition. This change of the dielectrophoretic force field must be due to the permittivity of the nanotube−surfactant hybrid being much larger than the aqueous solution.[16] For self-limiting single-nanotube deposition, it is critical that only one nanotube at a time enters the central region between the electrode gap. In our setup this is fulfilled at a nanotube concentration of no more than 5 nanotubes/μm^3 for an applied bias of 2.5×10^6 V/m. Higher nanotube concentration or electric field strength could attract and simultaneously deposit more than one nanotube in the gap. The small fraction of multiple-nanotube devices observed is attributed to such simultaneous deposition. The control over single-nanotube deposition is most robust with thicker oxides. For thin oxide, the underlying conducting substrate disturbs the electric field on the surface.[17] As such, the mechanism is not restricted to carbon nanotubes and should work equally well with nanowires or any polarizable one-dimensional object. Moreover, alternative wiring schemes besides capacitive coupling, such as direct contact to both electrodes, can also involve such self-limiting deposition.

Each of the devices thus fabricated can be individually addressed, as they have a common BE (source) but separate CEs (drain) and the underlying silicon substrate as a common third electrode (gate). This allows for three-terminal measurements of transport properties. The number of individual nanotube devices on a single chip is no longer the limiting factor in large-scale integration of nanotube devices. On the other hand, it provides a new challenge in having to individually connect each of these devices to the macroscopic world or to each other, in order to study their fundamental properties or to integrate them into logic circuits. In the as-deposited configuration, these arrays are ideally suited for nanotube-based sensor applications. As the precise location of each nanotube device is predetermined, it is now possible to use multiple levels of subsequent metallization in order to gain access to each individual device. Alternately, each device can also be accessed by commercial submicrometer probe systems.

To establish that the devices fabricated by the above procedure are in fact active and robust, we used submicrometer probes (Kammrath & Weiss "Pico Prober" Module) mounted inside a SEM to contact individual electrode pairs and measure the electronic transport through the nanotubes, as seen in Figure 5a. Over 100 pairs of bridged

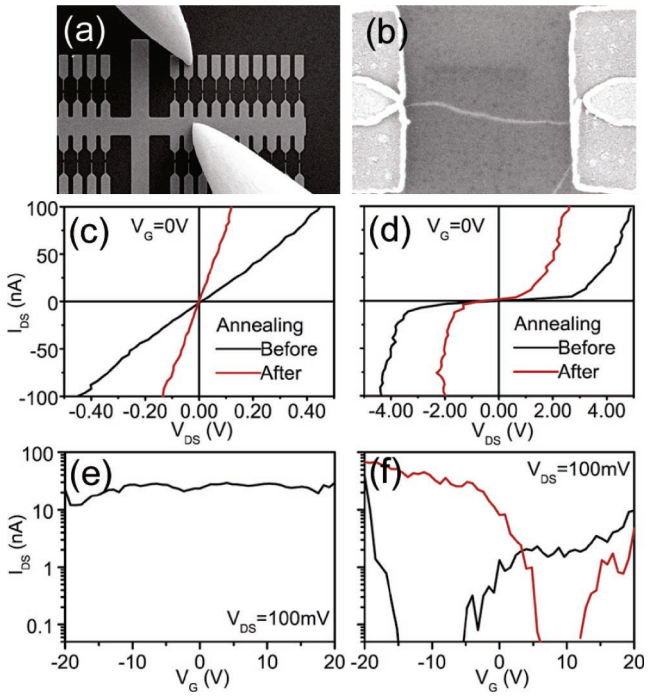

Figure 5. (a) Scanning electron micrograph of the high-density nanotube device array, with two in situ submicrometer probes (source and drain) contacting the electrodes for electronic transport measurements. (b) Scanning electron micrograph of a device after a second lithography, allowing the ends of the nanotube to be completely surrounded by metal for a reduced contact resistance. Electric transport characterization: (c, d) source−drain current (I_{DS}) vs voltage (V_{DS}) curves, (e, f) transfer characteristics, I_{DS} vs gate voltage (V_G) of representative metallic (c, e) and semiconducting (d, f) carbon nanotubes devices. Metallic nanotubes show typical linear $I-V$ and no gate-voltage dependence. Semiconducting nanotubes show nonlinear $I-V$ due to the Schottky barrier at the nanotube−metal contact and strong gate-voltage dependence. (c, d) Contact resistance before (black line) and after (red line) annealing at 200 °C for 2 h, significantly reduced after annealing. (f) Transfer characteristics of a semiconducting nanotube device, showing hysteresis between the forward (red) and reverse (black) sweeps of V_G. For statistics on contact resistance, see Supporting Information.

10 μm^2 electrodes were measured, and all of them turned out to be functioning devices, indicating the reliability of our fabrication technique. The 1 μm^2 electrodes, however, were too small to be probed with the same in situ submicrometer probes for electrical characterization. As expected, characteristics of both metallic and semiconducting nanotubes were observed, as the deposition frequency was well below the crossover frequency for electronic type specific nanotube separation. The current−voltage ($I-V$) characteristics and gate-voltage dependence of representative metallic and semiconducting devices are presented in Figure 5. Due to the nanotube-on-metal configuration, the contact resistances of these devices are initially high, generally 2−5 MΩ. However, the contact resistance can be significantly lowered by annealing the devices at 200 °C for 2 h.[18] After the devices were annealed, the contact resistance was typically 500 kΩ to 1 MΩ, as shown in Figure 5c−5f and Supplementary Figure 4a. This can be attributed to a combination of improved metal−nanotube interface and

desorption of residual surfactant from the nanotube surface. It is possible to further reduce the contact resistance by performing a second lithography step and metallization at the nanotube−metal junction region, to embed the ends of the nanotube in the contact metal (Pd), as shown in Figure 5b. This reduces the contact resistance of the nanotube devices to ≤100 kΩ (Supplementary Figure 4a) since Pd is one of the best-known metals for contacting nanotubes.[19] This of course is possible only because the nanotubes have now been assembled precisely at predefined locations, rather then being dispersed randomly across electrode pairs. Semiconducting nanotube devices also show excellent transistor characteristics, with high ON state conductances comparable to metallic nanotubes, and large ON/OFF ratios ($>10^3$), as shown in Supplementary Figure 4b.

The method described in this report is very versatile, as it can be used in conjunction with a variety of nanotube processing techniques such as nanotubes separated based on their electronic properties, length, diameter, or even chirality.[20−22] It is also compatible with postprocessing techniques like multiple layers of subsequent metallization to improve their contact properties, fabricate dedicated gate electrodes to each device, or make the individual devices accessible to the macroscopic world. Furthermore, this technique is not limited to nanotubes alone and could be extended to fabricate large-scale reliable contacts to other nanoscale objects such as nanowires, individual molecules, or biological entities such as DNA or cells.

In conclusion, we report a novel aspect of dielectrophoretic deposition of nanotubes, where the dielectrophoretic force field changes upon nanotube deposition and thereby self-limits the directed assembly to a single nanotube or nanotube bundle at predefined locations. The previously accepted mechanism for such self-limited assembly has been established in this report to be incorrect in the case of nanotubes, due to the unique contact properties of the nanotube−metal interface. By using this effect in combination with capacitively coupled counter electrodes, we demonstrate very high densities (greater than 1 million/cm^2) of individually contacted single-walled carbon nanotube devices, 3−4 orders of magnitude higher than was possible before.[23,24] The process is fully compatible with current microfabrication technologies, requires no chemical modifications of either the substrate or the nanotubes, and can be coupled with all forms of pre- and postprocessing of the nanotube and the substrate. The nanotubes form reliable contacts to the electrodes. This result takes nanotube electronic devices a big step closer to integrating with microelectronics and expanding its scope for commercial viability. On a laboratory scale, it now allows for the fabrication of a large number of devices with identical nanotube source and deposition conditions, to perform truly statistical measurements of nanotube properties like electronic transport or Raman mapping.

Acknowledgment. A.V. acknowledges the Alexander von Humboldt Foundation. R.K. and S.B. acknowledge funding by the Initiative and Networking Fund of the Helmholtz-Gemeinschaft Deutscher Forschungszentren (HGF). The authors acknowledge S. Dehm for assistance with electron-beam lithography.

Supporting Information Available: Descriptions of materials and methods including nanotube suspension and substrate, nanotube deposition, and electric field and field gradient simulation and figures showing optical absorption spectrum of SWNTs in aqueous surfactant solution, impedance spectroscopy measurements, simulated maps of potential distribution around the electrodes, and box plot of statistical distribution of the resistance and conductance of metallic nanotube devices. This material is available free of charge via the Internet at http://pubs.acs.org.

References

(1) Tans, S. J.; Devoret, M. H.; Dai, H.; Thess, A.; Smalley, R. E.; Geerligs, L. J.; Dekker, C. *Nature* **1997**, *386*, 474.
(2) Nygård, J.; Cobden, D. H.; Bockrath, M.; McEuen, P. L.; Lindelof, P. E. *Appl. Phys. A* **1999**, *69*, 297.
(3) Wei, B. Q.; Vajtai, R.; Ajayan, P. M. *Appl. Phys. Lett.* **2001**, *79*, 1172.
(4) Avouris, P. *Acc. Chem. Res.* **2002**, *35*, 1026.
(5) Bockrath, M.; Cobden, D. H.; McEuen, P. L.; Chopra, N. G.; Zettl, A.; Thess, A.; Smalley, R. E. *Science* **1997**, *275*, 1922.
(6) Kociak, M.; Kasumov, A. Y.; Guéron, S.; Reulet, B.; Khodos, I. I.; Gorbatov, Y. B.; Volkov, V. T.; Vaccarini, L.; Bouchiat, H. *Phys. Rev. Lett.* **2001**, *86*, 2416−2419.
(7) McEuen, P. L.; Fuhrer, M. S.; Park, H. *IEEE Trans. Nanotechnol.* **2002**, *1*, 78.
(8) Zhang, Y.; Chang, A.; Cao, J.; Wang, Q.; Kim, W.; Li, Y.; Morris, N.; Yenilmez, E.; Kong, J.; Dai, H. *Appl. Phys. Lett.* **2001**, *79*, 3155.
(9) Rao, S. G.; Huang, L.; Setyawan, W.; Hong, S. *Nature* **2003**, *425*, 36.
(10) Krupke, R.; Hennrich, F.; Weber, H. B.; Beckmann, D.; Hampe, O.; Malik, S.; Kappes, M. M.; Lohneysen, H. v. *Appl. Phys. A* **2003**, *76*, 397−400.
(11) Krupke, R.; Hennrich, F.; Weber, H. B.; Kappes, M. M.; Lohneysen, H. v. *Nano Lett.* **2003**, *3*, 1019−1023.
(12) Chung, J.; Lee, K.-H.; Lee, J.; Ruoff, R. S. *Langmuir* **2004**, *20*, 3011−3017.
(13) Liu, Y.; Chung, J.-H.; Liu, W. K.; Ruoff, R. S. *J. Phys. Chem. B* **2006**, *110*, 14098−14106.
(14) Andriotis, A. N.; Menon, M.; Froudakis, G. *Appl. Phys. Lett.* **2000**, *76*.
(15) Chen, Z.; Appenzeller, J.; Knoch, J.; Lin, Y.; Avouris, P. *Nano Lett.* **2005**, *5*, 1497.
(16) Krupke, R.; Hennrich, F.; Kappes, M. M.; Lohneysen, H. v. *Nano Lett.* **2004**, *4*, 1395−1399.
(17) Marquardt, C. W.; Blatt, S.; Hennrich, F.; Löhneysen, H. V.; Krupke, R. *Appl. Phys. Lett.* **2006**, *89*, 183117.
(18) Oron-Carl, M.; Hennrich, F.; Kappes, M. M.; Löhneysen, H. v.; Krupke, R. *Nano Lett.* **2005**, *5*, 1761−1767.
(19) Mann, D.; Javey, A.; Kong, J.; Wang, Q.; Dai, H. *Nano Lett.* **2003**, *3*, 1541.
(20) Heller, D. A.; Mayrhofer, R. M.; Baik, S.; Grinkova, Y. V.; Usrey, M. L.; Strano, M. S. *J. Am. Chem. Soc.* **2004**, *126*, 14567−14573.
(21) Arnold, M. S.; Green, A. A.; Hulvat, J. F.; Stupp, S. I.; Hersam, M. C. *Nat. Nanotechnol.* **2006**, *1*, 60−65.
(22) Krupke, R.; Hennrich, F. *Adv. Eng. Mater.* **2005**, *7*, 111−116.
(23) Lastella, S.; Mallick, G.; Woo, R.; Karna, S. P.; Rider, D. A.; Manners, I.; Jung, Y. J.; Ryu, C. Y.; Ajayan, P. M. *J. Appl. Phys.* **2006**, *99*, 024302.
(24) Javey, A.; Wang, Q.; Ural, A.; Li, Y.; Dai, H. *Nano Lett.* **2002**, *2*, 929−932.
(25) Homma, Y.; Suzuki, S.; Kobayashi, Y; Nagase, M.; Takagi, D. *Appl. Phys. Lett.* **2004**, *84*, 1750−1752.

NL0703727